Journal of Combinatorial Mathematics and Combinatorial Computing
www.combinatorialpress.com/jcmcc

Combinatorial Press

A Study on the Geometric Characteristics of Line Mobility and Structural Changes in the Aesthetic System of Chinese Calligraphy

Dong Wang[1,] ✉

[1,] *School of Fine Arts and Calligraphy, Nanjing University of the Arts, Nanjing, Jiangsu, 210013, China*

ABSTRACT

As an important part of Chinese traditional culture and art, how to efficiently realize the recognition, retrieval and style appreciation of calligraphy is of great significance. Aiming at the shortcomings of the traditional geometric feature recognition model with low recognition efficiency, this paper applies morphological neural network to the geometric feature recognition of calligraphy to design a geometric feature recognition model for calligraphy. Image enhancement is performed on the calligraphic graphics, the expansion pooling subnet is designed to replace the maximum pooling layer, and the calligraphic geometric feature recognition network is constructed by combining the residual block structure. The average recognition accuracy of this model in the geometric feature refinement recognition task is as high as 97.23%, which is higher than that of the comparative models such as CNN, LeNet-5, and the recognition accuracies are not less than 96% for the Euclidean, Liu, Zhao, and Yan styles. Using the model of this paper to explore the influence of calligraphic line fluidity and structural changes on the geometric features, it is analyzed that the "line" has a more significant influence on the geometric features of calligraphy than the "structure". In the six types of traditional calligraphy, such as large seal, small seal, official script, regular script, line script, and cursive script, cursive script is only similar to the geometric characteristics of line script, and the geometric characteristics are very unique.

Keywords: morphological neural networks, inflated pooled subnets, residual block structure, calligraphic geometric features

1. Introduction

Calligraphy in ancient times was mainly practical, and also had an appreciation function. Nowadays, the practicality of calligraphy has been greatly weakened, and the aesthetics has been greatly enhanced. With the development of the times, the overall economic level of the society has been improved, the overall knowledge and cultural level of the people has been improved, and the aesthetics has been gradually

✉ Corresponding author.
E-mail address: fantasy_jin@163.com (D. Wang).
Received 22 October 2024; Revised 19 December 2024; Accepted 18 February 2025; Published Online 15 April 2025.
DOI: 10.61091/jcmcc127a-137

diversified [1-4]. Chinese traditional aesthetics is composed of a series of categories that are rich in Chinese characteristics, and the colorful categories form the unique landscape of Chinese traditional aesthetics [5-6]. In this context, if calligraphy wants to develop further, it needs to sort out and scrutinize the unique aesthetic system and aesthetic theories in it, clarify the position of the aesthetics of calligraphy in the construction of the discipline of calligraphy, and bring into play the functions and roles of the aesthetics of calligraphy, so as to endow calligraphy with a wider space for development [7-9]. Discussing the aesthetics of calligraphy, we should first discuss the premise of its existence. With the continuous development of calligraphy, the aesthetic function and role of calligraphy is more and more prominent, the more prominent artistic attributes, calligraphy is also freed from the practicality of the fence, and become an art with aesthetic creation as the main goal [10-12]. Under the premise that "calligraphy is a kind of art", the aesthetics of calligraphy can help people to recognize and appreciate calligraphy in the long history of art [13-14]. The study of the geometric characteristics of line fluidity and structural changes in the aesthetic system of Chinese calligraphy not only helps to guide the current practice of calligraphy, but also provides a new perspective of thinking and elaboration for the study of the theory of calligraphy, and plays a positive role in the establishment of a complete and systematic calligraphy theory system, which is irreplaceable and guiding significance for people to scrutinize the tradition of calligraphy and to think about the future direction of calligraphy [15-19]. The book is a great example of how the Chinese calligraphy tradition can be utilized in the future.

In order to realize the efficient recognition of Chinese calligraphy combined with features, this paper takes morphological convolutional neural network as the basis to design the recognition model of calligraphic geometric features. Image enhancement is performed on the original dataset of collected Chinese calligraphy characters to construct a complex expanded dataset. The morphological convolutional neural network for calligraphy geometric feature recognition is designed and constructed through the morphological neural network design expansion pooling subnet with E-D structure and D-E structure, combined with the residual block structure design, and the training of the combined feature recognition network is carried out to realize the improvement of the accuracy of calligraphy geometric feature recognition. On the TensorFlow framework platform, several comparison experiments are carried out on the model of this paper to verify the effectiveness of the model. Using the model of this paper to deeply explore the influence of line fluidity and structural changes on the geometric structural features of calligraphy.

2. Chinese Calligraphy Geometric Feature Recognition Model

2.1. *Mathematical Morphology Filter*

As the most basic concept in mathematical morphology, mathematical morphological operators can be used to extract features in data and filter noise in data. Since the vibration signals of bearings are one-dimensional data, this paper only discusses the mathematical morphology filter theory for one-dimensional data [20].

Let $f(n)$ be a one-dimensional signal on set $F=\{1,2,\cdots,n-1\}$ and $g(m)$ be a structural element (SE) on set $G=\{1,2,\cdots,m-1\}$ that satisfies $n\geq m$. The basic operators of mathematical morphology include the erosion operator, the expansion operator, the open operator, and the closed operator, and all morphological operators evolve from these four basic operators. The basic definitions of the four operators are as follows:

$$(f\Theta g)(n)=\min_{m\in G}\{f(n+m)-g(m)\} \tag{1}$$

$$(f\oplus g)(n)=\max_{m\in G}\{f(n-m)+g(m)\} \tag{2}$$

$$(f\circ g)(n)=(f\Theta g\oplus g)(n) \tag{3}$$

$$(f\cdot g)(n)=(f\oplus g\Theta g)(n) \tag{4}$$

Where formula (1) is the morphological erosion operator and formula (2) is the morphological expansion operator. Equation (3) is the open operator and equation (4) is the closed operator. The corrosion operator is usually used to smooth the negative impulse component of the signal and suppress the positive impulse component of the signal. The expansion operator has the opposite function of the erosion operator. The expansion operator is often used to smooth the positive impulse components in a signal and suppress the negative impulse components in a signal. The morphological open and morphological closed operators are defined as a cascade of corrosion and expansion operators that can process both positive and negative impulse components in a signal. A signal processed by the open operator has its image contracted to some extent. A signal processed by the closed operator will have its image expanded to some degree. Morphological open and morphological closed operators are effective in filtering the positive and negative impulse components of a signal. The impulse features of a signal contain information related to the impulse peaks of the signal and are very helpful in analyzing the signal. Therefore, it is extremely necessary to extract the impulse features of the signal. Top-hat operators are commonly used to mine positive and negative impulse features in signals, and top-hat operators include white top-hat operator (WTH) and black top-hat operator (BTH). The white top hat operator and black top hat operator are defined as follows:

$$WTH(f(n),g) = f(n) - (f \circ g)(n) \tag{5}$$

$$BTH(f(n),g) = (f \cdot g)(n) - f(n) \tag{6}$$

Equation (5) is the white top hat operation, which is often used to extract the positive pulse features in the signal. Equation (6) is the black top hat operation, which is commonly used to extract the negative pulse features in the signal.

According to the above discussion, the open operator can effectively filter the positive impulse components in the signal, while the closed operator is exactly the opposite. Many filtering operators are constructed on the basis of open and closed operators, and two commonly used filtering operators are given below:

$$F_{OC}(f(n),g) = (f \circ g \cdot g)(n) \tag{7}$$

$$F_{CO}(f(n),g) = (f \cdot g \circ g)(n) \tag{8}$$

Where Eq. (7) is the morphological open and closed operator and Eq. (8) is the morphological closed-open operator. These two operators can filter the positive and negative pulse components in the signal at the same time, however, the amplitude of the signal will become smaller after the processing of F_{OC}, and the amplitude will become larger after the processing of F_{CO}. So these two operators are not suitable to be used directly for noise reduction of signals. The Combined Morphological Filter (CMF) solves this problem well by calculating the arithmetic mean of the two operators.The CMF operator is defined as follows:

$$CMF(f(n),g) = \frac{F_{OC}(f(n),g) + F_{CO}(f(n),g)}{2} \tag{9}$$

Also commonly used mathematical morphological operators include morphological gradient operators, which combine various basic morphological operators through difference operations to achieve filtering effects. The expressions of several common morphological gradient operators are as follows:

$$MG(f(n),g) = (f \oplus g)(n) - (f \Theta g)(n) \tag{10}$$

$$MG_{CO}(f(n),g) = (f \cdot g)(n) - (f \circ g)(n) \tag{11}$$

$$MG_{COOC}(f(n),g) = F_{CO}(f(n),g) - F_{OC}(f(n),g) \tag{12}$$

At present, for various scenarios that require filtering, experts and scholars at home and abroad have proposed many morphological operators with stronger noise reduction performance, but these

morphological operators are basically combinations of the commonly used morphological operators mentioned above.

The optimal lengths of the structural elements of single-scale morphological filters are usually difficult to determine, and the practice of processing signals only on a single scale is prone to lose important feature information in the signals. Multiscale morphological filters compensate for the shortcomings of single-scale morphological filters to some extent. In multiscale morphology, the lengths of the structural elements are variable over a range. This allows the filter to filter the noise in the signal at different resolutions, preventing the loss of useful information in the signal during the noise reduction process. In multiscale morphology, the definition of multiscale structural elements is as follows is defined below:

$$\lambda g = \underbrace{g \oplus g \oplus g \cdots \oplus g}_{\lambda - 1} \tag{13}$$

where λ is the scale factor and g is the structural element at a single scale. Equation (13) shows that the analyzed scale size of λ is obtained by expanding the single scale structural element $\lambda - 1$ times. As λ increases, the length of λg increases. At the same time the coverage of the original signal by the multi-scale structural elements increases. It can be seen that in multiscale morphology, the morphological operators analyze the signal more comprehensively and are no longer limited to analyzing only a single scale. In this respect multiscale morphological filters have surpassed many conventional filters.

In multiscale morphology, the representation of morphological operators needs to be rewritten. Taking the morphological corrosion operator and the morphological expansion operator as examples, the expression forms of the two operators in multiscale morphology are as follows:

$$f \Theta \lambda g = (f \Theta g \Theta g \Theta \cdots \Theta g)(n) \tag{14}$$

$$f \oplus \lambda g = (f \oplus g \oplus g \oplus \cdots \oplus g)(n) \tag{15}$$

where Eq. (14) is the multiscale morphological erosion operation and Eq. (15) is the multiscale morphological expansion operation. Multiscale mathematical morphology usually integrates each scale of analysis in a weighted manner, and the weighted multiscale morphological filter (WMMF) is defined as follows:

$$WMMF(f(n), g) = \sum_{\lambda} \omega_{\lambda} Operator_{\lambda}(f(n), g) \tag{16}$$

where $Operator(f(n), g)$ is the multiscale morphological operator at analysis scale λ and ω_{λ} is the weight for that analysis scale.

2.2. Morphological neural network modeling

2.2.1. Morphological Neural Network Framework. CMNN is developed from the morphological perceptron model, which constructs two hyper-box clusters to realize binary classification. And CMNN is a combination of a series of morphological perceptron, which constructs m super-box cluster m as the number of classifiers and realizes multi-classification.

The minimum hyperbox $[a,b]$ covering the point set $C = \left\{ x_i \mid x_i \in G^n, i = 1,2,\cdots,k \right\}$ and its lower endpoint a and upper endpoint b are easily defined according to the theory of lattice algebra:

$$a = \left(\wedge x_i^1, \wedge x_i^2, \cdots, \wedge x_i^n \right) i = 1,2,\cdots,k \tag{17}$$

$$b = \left(\vee x_i^1, \vee x_i^2, \cdots, \vee x_i^n \right) i = 1,2,\cdots,k \tag{18}$$

When $n \le 3$, the hyperbox has an image geometric meaning. A certain vector $x \in G^n$ is contained in the hyperbox $[a,b]$, i.e., it satisfies $a \le x \le b$. The above condition is equivalent if we let $v = a^*$, $w = b$:

$$\varepsilon_v(x) \wedge \overline{\delta}_w(x) \ge 0 \tag{19}$$

Let the CMNN input vector be $x \in G^n$ and the output vector be $y \in G^m$. Given a set of training samples C, during the training process of the CMNN, a cluster of super-boxes $\left[a_1^j, b_1^j\right](j=1,2,\cdots,l_1)$ containing only the first type of training samples is automatically generated by the computation of morphological operators ε, $\overline{\delta}$ denoted as B_1, l_1 as the number of super-boxes in super-box cluster B_1. Then $B_2=\left[a_2^j, b_2^j\right](j=1,2,\cdots,l_2)$, l_2 are generated as the number of superboxes in superbox cluster B_2. This continues until $B_m=\left[a_m^j, b_m^j\right](j=1,2,\cdots,l_m)$, l_m are produced as the number of superboxes in superbox cluster B_m. It can be seen that not only does the number of hidden layer neurons of the CMNN not need to be determined manually, but also the number of constructed hidden layer neurons may not be equal for different morphological perceptrons.

For CMNN classification, for a given input sample $x \in G^n$, if it can be determined that x is contained in a certain hyperbox $\left[a_i^j, b_i^j\right](i=1,2,\cdots m: j=1,2,\cdots,l_i)$, i.e., belongs to a certain cluster of hyperboxes B_i, then it is determined that x belongs to class i.

2.2.2. Morphological Neural Network Multi-Classification Training Algorithm. To facilitate the description of the training algorithm for morphological neural networks, the concept of half-spaces, i.e., negative half-space $H_i^-(c)$ and positive half-space $H_i^+(c)$, is first introduced, and set $x, c \in L^n$, then defined:

$$\begin{aligned} H_i^-(c) &= \left\{x \in L^n : x_i < c_i\right\} i=1,2,\cdots,n \\ H_i^+(c) &= \left\{x \in L^n : x_i > c_i\right\} i=1,2,\cdots,n \end{aligned} \tag{20}$$

where subscript i is the dimension index of vectors x, c.

As mentioned earlier, the hyperbox has a figurative geometric meaning when $n \le 3$. When $n=2$. The small circles in the figure represent the samples of class i, the asterisks represent all the samples except class i. The geometric images of the point set, the half-space, the minimal hyperbox A_i^1 covering the point set of class i and its lower endpoints a_i^1 and upper endpoints b_i^1 are clearly represented in the figure.

Problem Description, Let the set of training samples be $C=\left\{x_1, x_2, \cdots, x_t\right\} \subset G^n$ and the sample set C contain a total of m classes of samples. It is necessary to find a training algorithm for the morphological neural network such that the trained network produces m clusters of hyperboxes $B_1, \cdots, B_m$, where $B_i=\left\{\left[a_i^1, b_i^1\right], \left[a_i^2, b_i^2\right], \cdots, \left[a_i^{l_i}, b_i^{l_i}\right]\right\}$ ($i=1,2,\cdots,m$, l_i is the number of hyperboxes contained in B_i) is the set of hyperboxes containing all the training samples of class i.

Morphological neural networks cannot be trained by traditional back propagation algorithms, both Sussner P and Li Bing proposed binary classification training algorithms, and this thesis here directly gives similar multiclassification CMNN training algorithms.

The training sample set C contains a total of m classes of training samples, and the following operations are done for the i th class of samples (i initial value is 1).

In the first step, initialize the super-box cluster $B_i=\varnothing$ to find out all the class i samples and put them into the operation sample set CI.

In the second step, the smallest hyperbox $A_i^1=\left[a_i^1, b_i^1\right]$ containing the sample set CI is computed by equations (18) and (19).

In the third step, find the non-class i samples covered under hyperbox $A_i^1=\left[a_i^1, b_i^1\right]$ by equation (20), denoted as C2C.

In the fourth step, determine whether C2C is empty. If the set C2C is empty, add the superbox A_i^1 to the superbox cluster B_i. The algorithm has converged for the i rd class of samples, the construction of

the superbox cluster containing the i th class of samples is complete, and the construction of the superbox cluster for the next class of samples begins, with the value of i added to one, from the first step. If the set C2C is not empty, the next step is executed.

In the fifth step, the smallest hyperbox $A=[c,d]$ covering the sample set C2C is computed from equations (18) and (19).

In the sixth step, compute the n negative half-space of c and the n positive half-space of d:

$$\begin{aligned} H_k^-(c)&=\{x\,|\,x_k<c_k, x\in CI\}\,k=1,2,\cdots,n\\ H_k^+(d)&=\{x\,|\,x_k>d_k, x\in CI\}\,k=1,2,\cdots,n \end{aligned} \tag{21}$$

In the seventh step, determine whether these half-spaces are empty or not, if a half-space is not empty, compute the smallest hyperbox A_i^j covering the half-space by Eqs. (18) and (19), and add it to the hyperbox cluster B_i.

In the eighth step, find out the i th class of samples covered under the hyperbox $A=[c,d]$ by Eq. (20), denoted as C1C.

In the ninth step, determine whether C1C is empty. If the set C1C is empty, it means that the algorithm has converged for the first i class of samples, the construction of the first i class of samples super-box clusters is completed, and the construction of the next class of samples super-box clusters is started, and the i-value is added to one, which is executed from the first step. If the set C1C is not empty, the next step is executed.

In the tenth step, make $CI=C1C$ and go to the second step to start the execution.

From the above steps, it can be seen that the process of training the samples of class i is the process of constructing the hyperbox clusters B_i step by step, and also the process of operating the sample set CI to collect the clusters to the center continuously. After executing all m classes of training samples, the whole algorithm closes the clusters and constructs m super-box clusters. At this point the morphological network has been trained and can be used to classify the test samples.

The network training process constructs the clusters of each hyperbox while finding a hypercube covering all samples. First, the minimum hyperbox $B_r=[e,f]$ covering all the samples is easily found from equations (18) and (19), and a hypercube is constructed with the lower endpoint e of B_r as the lower endpoint and the maximum side length of the hyperbox B_r as the side length $B=[e,u]$. This hypercube is a parameter that will be used in calculating the inclusiveness measure.

2.2.3. Computational output model for morphological neural networks. Expressed in mathematical language, for a given input sample $x\in G^n$, the output y_i of the i nd morphological perceptron is denoted as:

$$y_i=f\left(\bigvee_{j=1}^{l_i}\left(\varepsilon_{v_i^j}(x)\wedge\overline{\delta}_{w_i^j}(x)\right)\right) \tag{22}$$

where the hard threshold function:

$$f(x)=\begin{cases}1 & x\geq 0\\ 0 & x<0\end{cases} \tag{23}$$

From equations (21) and (22), x is classified as class i when $y_i=1$.

However, for a given sample x, if x is not contained in any of the known hyperboxes, then the value of $\varepsilon_v(x)\wedge\overline{\delta}_w(x)$ is always less than zero and the classification fails. Therefore for classification, y_i is obtained directly by the following equation:

$$y_i=\bigvee_{j=1}^{l_i}\left(\varepsilon_{v_i^j}(x)\wedge\overline{\delta}_{w_i^j}(x)\right) \tag{24}$$

After calculating the output $y_i(i=1,2,\cdots,m)$ of each morphological perceptron in the CMNN, x is classified to the class with the largest output value according to the principle of maximum affiliation.

2.3. *Calligraphic Geometric Feature Recognition Model*

In this section, we will construct a calligraphy geometric feature recognition model based on mathematical morphological filters, combined with morphological operators to study the depth of morphological convolutional neural network MCNN to improve the accuracy of calligraphy style recognition [21].

2.3.1 Image expansion based on Chinese character glyphs. This section expands the calligraphic images by performing affine transform, noise transform and inverse transform on the original dataset to simulate the acquisition process in a real environment.

1) Affine transformations [22]. Affine transformations utilize linear transformations and geometric translations to accomplish the transformation of one vector space to other vector spaces. This method is able to utilize the transformation matrix to complete four transformations: translation, rotation, scaling and miscutting. The translation and rotation transformations do not change the shape and size of the image, and for the two-dimensional coordinate point (x,y), the transformation is represented as (u,v), and the chi-square coordinate matrices of the two are shown in Eqs. (25) and (26), respectively:

$$\begin{bmatrix} u \\ v \\ 1 \end{bmatrix} = \begin{bmatrix} 1 & 0 & t_x \\ 0 & 1 & t_y \\ 0 & 0 & 1 \end{bmatrix} \begin{bmatrix} x \\ y \\ 1 \end{bmatrix} \tag{25}$$

$$\begin{bmatrix} u \\ v \\ 1 \end{bmatrix} = \begin{bmatrix} \cos\theta & -\sin\theta & 0 \\ \sin\theta & \cos\theta & 0 \\ 0 & 0 & 1 \end{bmatrix} \begin{bmatrix} x \\ y \\ 1 \end{bmatrix} \tag{26}$$

where t_x and t_y are translation vectors and θ is the rotation angle.

The scaling transform is the image scaling relative to the origin, if the coefficient is negative it will be flipped, the scaling coefficients along the x and y axes are denoted by S_x and S_y, and the representation of the scaling transform is shown in Equation (27):

$$\begin{bmatrix} u \\ v \\ 1 \end{bmatrix} = \begin{bmatrix} S_x & 0 & 0 \\ 0 & S_y & 0 \\ 0 & 0 & 1 \end{bmatrix} \begin{bmatrix} x \\ y \\ 1 \end{bmatrix} \tag{27}$$

The miscut is divided into horizontal and vertical directions for the miscut transformation, using matrices T_1 and T_2 to represent the miscut transformation matrices in the horizontal and vertical directions, respectively, and α and β are the miscut angles, then the transformation matrices T_1 and T_2 are shown in Eq. (28):

$$T_1 = \begin{bmatrix} 1 & \tan\alpha & 0 \\ 0 & 1 & 0 \\ 0 & 0 & 1 \end{bmatrix}, T_2 = \begin{bmatrix} 1 & 0 & 0 \\ \tan\beta & 1 & 0 \\ 0 & 0 & 1 \end{bmatrix} \tag{28}$$

2) Noise Transformation. Image noise can be viewed as extra pixel points or blocks of pixels produced by random variables in its transmission [23]. Three common types of noise, Gaussian noise, pretzel noise and speckle noise are described below, where x denotes the gray value variable.

The probability density function of Gaussian noise obeys a Gaussian distribution with a mean of μ and a variance of σ^2. The probability density function of Gaussian noise is shown in Equation (29):

$$f(x)=\frac{1}{\sqrt{2\pi}\sigma}e^{\frac{-(x-\mu)^2}{2\sigma^2}} \tag{29}$$

Pepper noise is the noise caused by the intensity of the signal pulse, also called impulse noise, which is presented as a stray dot on the image, and the expression of the probability density function is shown in Eq. (30):

$$f(x)=\begin{cases} f_a & x=a \\ f_b & x=b \\ 1-f_a-f_b & Other \end{cases} \tag{30}$$

Speckle noise is a type of image noise based on the correlation principle, which has a rougher reflective surface on the wavelength scale and therefore produces speckle after image processing.

3) Inverse transform. The inverse transform is a gray scale transformation that inverts the gray scale values of an image as shown in equation (31):

$$f_{ij}^{'}=255-f_{ij} \tag{31}$$

Most of the calligraphy works are black characters on a white background, but in some inscriptions, the calligraphic Chinese characters show different forms, such as white characters on a black background, so it can be realized by taking the inverse transformation.

2.3.2 Network design for recognition of calligraphic geometric features. In this section, we first design the inflated pooling subnetwork to replace the maximum pooling layer based on the $E-D$-structure and $D-E$-structure morphological neural networks, and then construct a morphological convolutional neural network for calligraphic geometric feature recognition in conjunction with the residual block structure design.

1) Design of expansion pooling subnetwork. The process of maximum pooling to select the maximum value can be regarded as a pooling operation carried out by an expansion operator with rectangular structural elements, so the operation process of the expansion operator can replace the operation of the maximum pooling layer, which not only reduces the loss of information, but also enhances the ability to extract features.

2) Style recognition network design. The calligraphy geometric feature recognition network MCNN constructed in this paper consists of an input layer, a convolutional layer, an expansion pooling subnetwork, four convolutional blocks, a fully connected layer and an output layer.

The parameter settings of the calligraphy geometric feature recognition network MCNN are described in detail below.

(1) Set the input image as a grayscale image of 128×128.

(2) The convolution kernel size of the convolution layer after the input layer is set to 7×7, and the number of channels is set to 64, the step size is adjusted to 2, and the SAME filling is used to better preserve the calligraphic geometric feature characteristics, and finally, the features are subjected to BN processing.

(3) The four convolutional blocks are named Conv1, Conv2, Conv3, and Conv4. The Conv1 convolutional block consists of three identical BasicBlock residual blocks, each of which contains two 3×3 -convolutional layers, each of which has 64 channels and a step size of 1, and is same-filled with the Relu activation function, followed by the BN process.Conv2 convolution block consists of four residual blocks, in which the first residual block includes two 3×3 convolutional layers and one 1×1 convolutional layer, with a step size of 2, 1, 2, respectively, and the remaining three residual blocks include two 3×3 convolutional layers, with a step size of 1, and the number of channels of all the residual blocks is 128. The Conv3 convolution block consists of six residue blocks, where the first residue block consists of two 3×3 -convolution layers and one 1×1-convolution layer, with steps of 2, 1, and 2, respectively, and the remaining five residue blocks consist of two 3×3-convolution layers, with a step of 1, and all the residue blocks have a channel count of 256. While the Conv4 convolution block consists of three residue blocks, where the first residue block consists of two 3×3-convolution layers and one 1×1-convolution layer with

the step size of 2, 1, and 2, respectively, and the remaining two residue blocks both consist of two 3×3-convolution layers with the step size of 1, and all of them have the number of channels in the residue block of 512.

(4) The fully connected layer integrates the features and retains 512 neurons.

(5) The output layer uses Softmax function for classification and recognition, 5 styles of calligraphy are 5 classification tasks, so the number of neurons is set to 5, which can complete the construction of the network to recognize the geometric features of calligraphy.

2.3.3 Calligraphy Geometric Feature Recognition Network Training. After setting the training parameters of the network, the network is trained and the training steps are as follows.

1) According to the geometric characteristics of five kinds of calligraphy, including regular script, seal script, cursive script, line script and official script, the training set was divided into five training subsets. The corresponding labels of the images in each subset are $[0,1,2,3,4]$, and all the image labels are encoded separately.

2) Initialize the number of iteration rounds to t, the maximum number of iteration rounds to T, $T\geq50$, and the current network model to H_t, and let $t=0, H=H_t$.

3) The 32 training samples randomly selected from the training sample set are used as inputs to the current recognition network model H_t to speed up the update rate of the weights and effectively reduce the network training time and the memory occupied by the network operation. The convolutional layer, the inflated pooling sub-network and the convolutional block perform feature extraction and filtering on each training sample to form the set of feature maps $F=\{f_1,f_2,\ldots,f_q,\ldots,f_{32}\}$. The fully-connected layer integrates the pixels of each feature map f_q into 512 pixel values. The 512 pixels obtained from the fully connected layer are mapped into 5 pixel values in the output layer, and the 5 pixel values are mapped into the predicted probability of each training sample belonging to each of the 5 calligraphic geometric feature classes by means of the Softmax function.

4) Using the cross-entropy loss function, calculate the loss value L_t of the current recognition network H_t by the predicted probability of each training sample belonging to the style category and the sample category label. Using the Adam optimization algorithm, the learning rate is set to 0.001, and the weights ω_t and deviations θ_t of the structural elements, convolutional and fully connected layers in the network H_t are updated by the loss value L_t, so as to obtain the network after the current selection of generation.

5) Judge whether $t\geq T$ is valid, if yes, get the trained network model H', otherwise, make $t=t+1$, and perform step 3).

3. Calligraphic Geometric Feature Recognition Test

In order to verify the feasibility of the improved calligraphic geometric feature recognition model in this paper for the recognition of calligraphic geometric features, several experimental comparisons of the model were conducted on the TensorFlow framework platform. A batch gradient descent algorithm is used to iteratively update the model parameters with batch=50, which traverses all the training set once every 48 iterations, i.e., one epoch. The calculation of training recognition rate and test recognition rate is carried out once per iteration, and the test recognition rate of this paper's model at different learning rates is specifically shown in Fig. 1. It can be seen that the convergence speed is different under different learning rates, the learning rate is too small will make the convergence speed too slow, the learning rate is too large will appear to skip the optimal value and can not reach the convergence, and finally the learning rate of this experiment is set to 0.001.

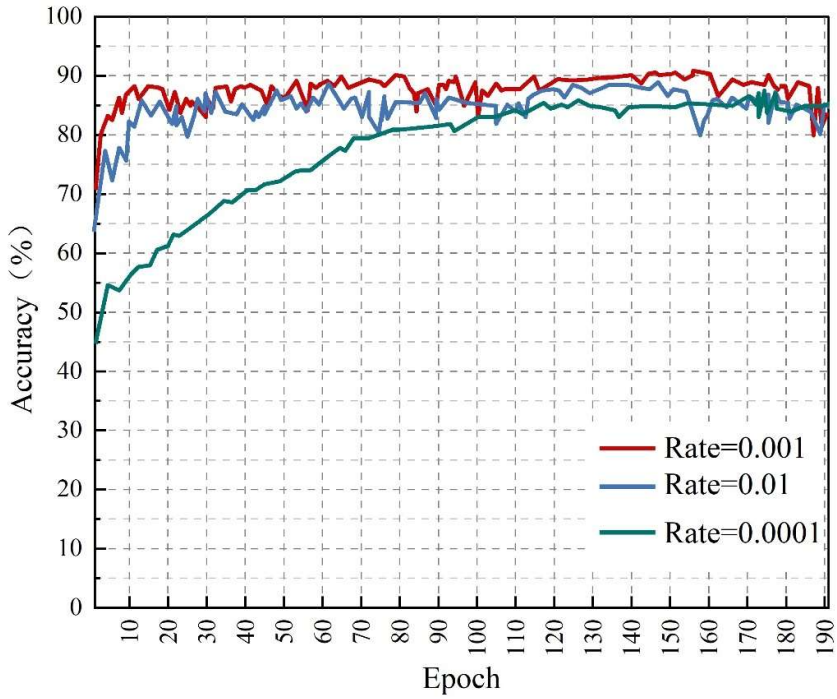

Fig. 1. Recognition rate on test

The function loss in the training process is getting smaller and smaller, that is, the loss function value reaches convergence at the smallest time, but in fact, it is necessary to keep the loss function value at a lower value for a period of time without jumping before it is considered to reach the basic convergence, and the trend of the function loss value in the training process under different learning rates is shown in Fig. 2, which shows that the rate of change of the loss value will be different under different learning rates, and choosing the appropriate learning rate will Selecting the appropriate learning rate helps the training to converge quickly.

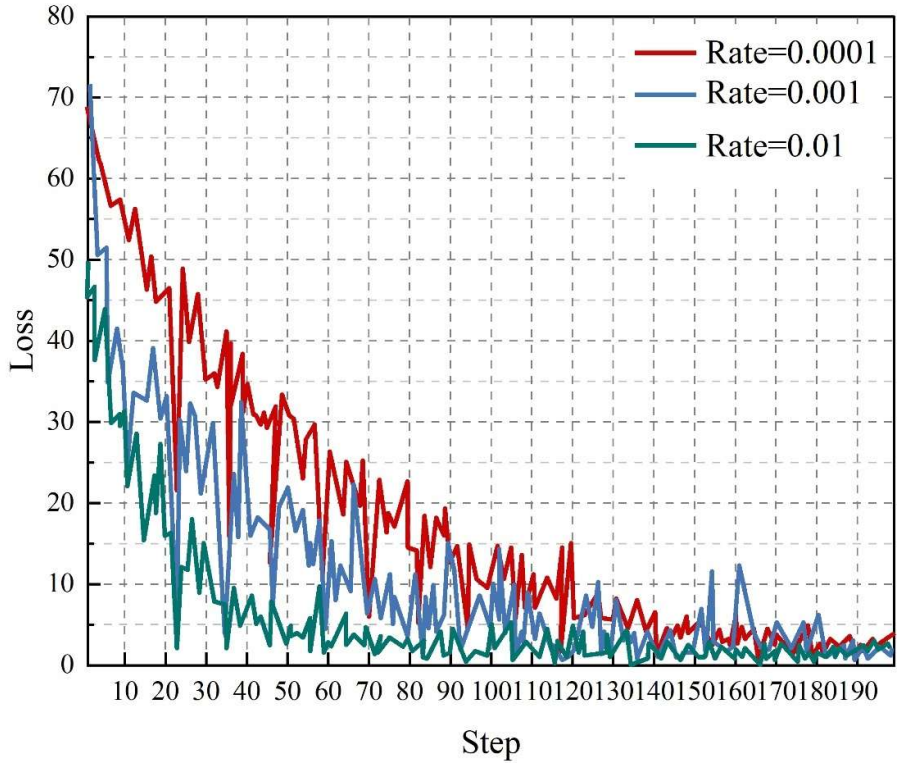

Fig. 2. The change of function loss value

Next, the task of applying the model of this paper to the recognition of calligraphic geometric feature refinement will be carried out, and CNN, LeNet-5, GoogLeNet, and ResNet models are selected as comparisons. Cross-experimentation of the five recognition models is carried out on the ancient regular script calligraphy dataset, and the parameters are updated iteratively and the accuracy is tested during the training process of the network model, and the recognition accuracy data is specifically shown in Table 1. One group (ABC/D, i.e., D is the test set, and the other ABC three groups are the training sets) test set D. Specifically, the average recognition accuracy of this paper's model is as high as 97.23%, which is 3.88%, 6.48%, 5.68%, and 0.78% higher than that of CNN, LeNet-5, GoogLeNet, and ResNet models. It has a relatively outstanding performance on the task of calligraphic geometric feature recognition, and it is also able to show a very high recognition rate on the task of calligraphic geometric feature refinement recognition.

Table 1. Data of recognition accuracy

Train/Test	CNN	LeNet-5	GoogLeNet	ResNet	Model of this article
ABC/D	84.78%	90.69%	90.13%	96.58%	97.36%
ABD/C	83.77%	89.93%	92.42%	96.37%	97.10%
ACD/B	81.92%	91.55%	91.81%	96.49%	97.34%
BCD/A	82.92%	90.82%	91.84%	96.35%	97.12%
Average	83.35%	90.75%	91.55%	96.45%	97.23%

In order to further analyze and study the recognition accuracy of the model proposed in this paper, the confusion matrix of cross-validation set on a set of ancient regular script calligraphy dataset is calculated, as shown in Fig. 3. It can be seen that the recognition accuracy of Ou style (Ouyang Xun) is the highest, with 99.8% being correctly recognized as Ou style, but there is still 0.2% that will be incorrectly recognized as Liu style (Liu Gongquan). Zhao Style (Zhao Mengfu) has the lowest recognition accuracy of 96%, with 2.5% being misidentified as Liu Style, 0.05% as Yan Style (Yan Zhenqing), and 1% as European Style. The other two fonts were also misidentified as other fonts. Some calligraphic character images are indeed very similar between the four calligraphic styles being difficult to distinguish. However, the vast majority of calligraphic characters can be recognized as the correct calligraphic style in the model of this paper. Therefore, the convolutional neural network model proposed in this paper can well accomplish the task of recognizing the refined styles of ancient regular script calligraphy refinement refinement and achieve the expected results.

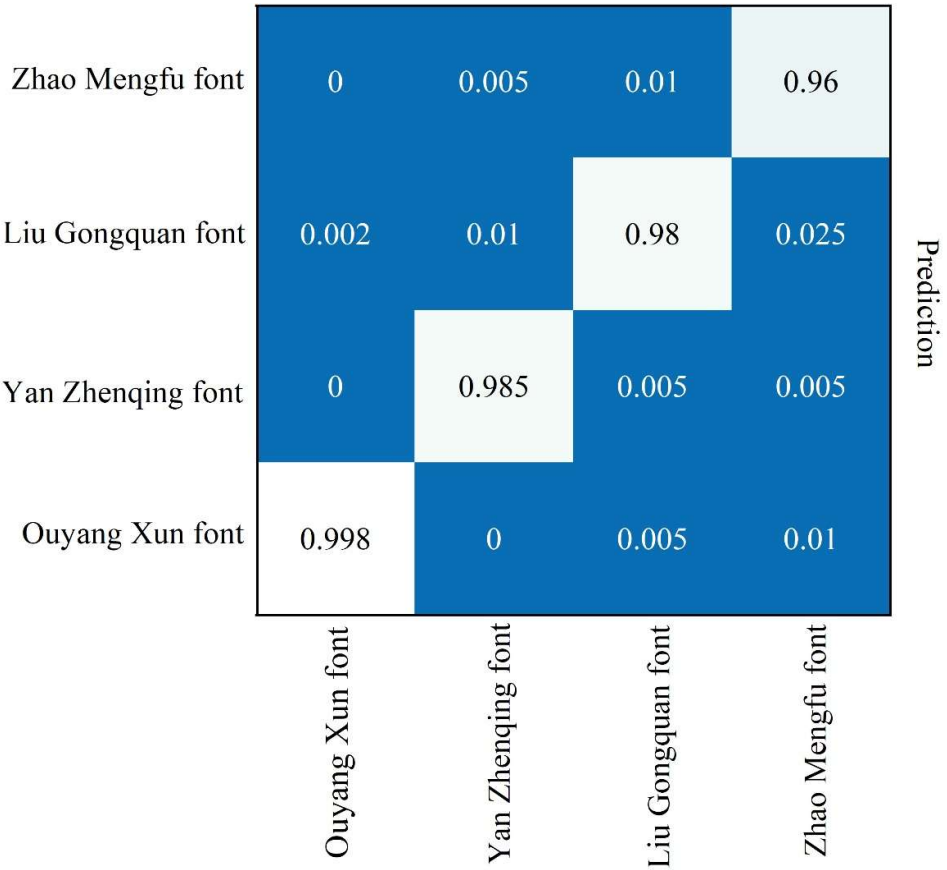

Fig. 3. Mixing matrix

4. Analysis of the influence of calligraphic lines and structure on geometric features

As the core features of calligraphic geometric features, calligraphic line and calligraphic structure are the roots and bones of calligraphy. This chapter will use the geometric feature recognition model of Chinese calligraphy constructed in this paper as the basis and means to explore the influence of line fluidity and structural changes on the geometric feature style of calligraphy in the aesthetic system of Chinese calligraphy.

Based on the classification of line and brushwork in the book style, this experiment selected 6 kinds of calligraphy (P1~P6 in turn) (P1~P6) were selected in this experiment, namely the calligraphy structure "original", "chapter unity", "strokes", and "one" (called S1~S4 in turn), as follows.

1) Original, i.e., intercepted from the original high-definition artwork.

2) Uniformity of chapters, i.e., based on the "Original" group of works, the layout of chapters is removed, and the characters are randomly sorted.

3) Strokes, i.e., from the "Works" group, appropriate Chinese characters are selected, the font structure is removed, and only the stroke structure of the Chinese characters is retained.

4) One, i.e., from the samples in the "works" group, select suitable Chinese characters, remove all the structures, and retain only the most basic structure of the horizontal shape.

This experiment will be a two-factor experiment, setting up a total of 24 experimental groups of calligraphic lines (6 styles of calligraphy) × structures (4 display styles), and collecting 600 valid data for each group with the help of the calligraphic geometric feature recognition model in this paper.

4.1. Cluster Analysis of Calligraphic Lines and Structural Hierarchy

Based on the Euclidean distance, the hierarchical clustering analysis of the brushwork structure was carried out, as shown in Figure 4. The darker the color in the diagram (the darker the blue), the closer the distance,

i.e., the more similar they are. Firstly, the clustering results were observed, and the structure was basically clustered according to the structure splitting process. In terms of calligraphy, the calligraphy is basically clustered according to the evolution process of the calligraphy, among which the large seal, small seal, official script and regular script are more clustered, and the line script is more similar to cursive script, which is also more in line with the traditional calligraphy theory. Observing the distance between the structure and the calligraphy lines, it is found that the distance between the large seal, the small seal, the official script and the regular script is closer to the four types of calligraphy structures, and the distance between the line and cursive script and the four types of calligraphy structure is farther.

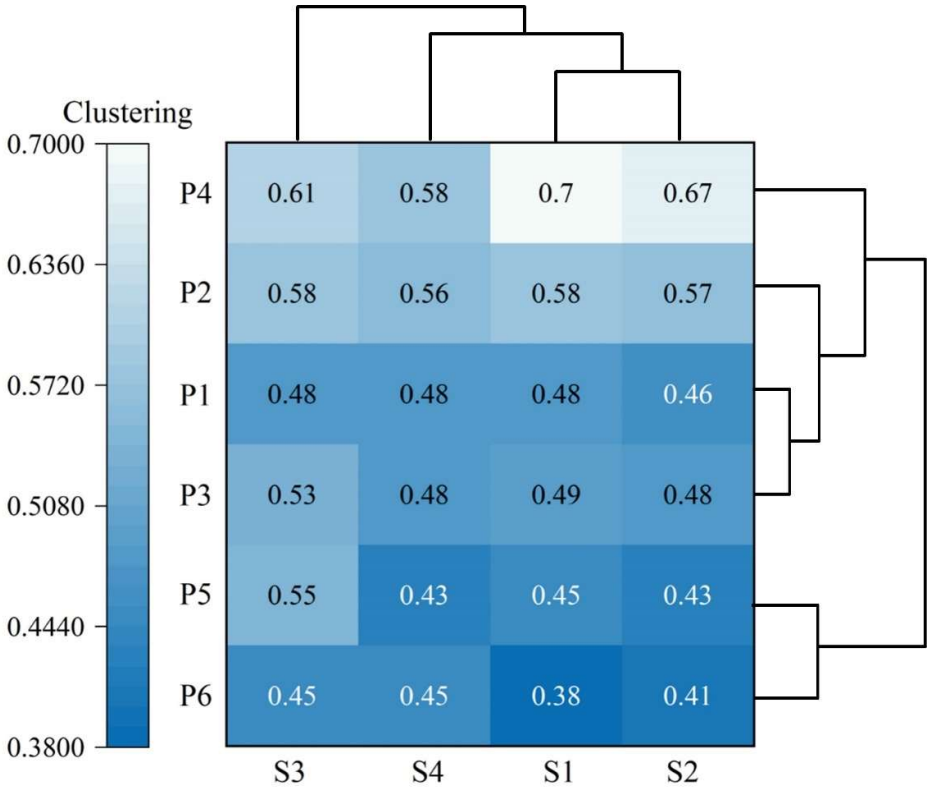

Fig. 4. Hierarchical clustering

4.2. Analysis of the correlation between calligraphic lines and structures

4.2.1. Analysis of the overall correlation between calligraphic line and structure. Figure 5 shows that Figure (a) is the similarity of the calligraphic structure and Figure (b) is the similarity between the calligraphic lines. As can be seen from Figure (a), the similarity between the structures is generally high, and the similarity between the structures is basically maintained at a high level except for the "one" group. Compared with the correlation between structures, (b) shows the diversity of perceptions brought about by calligraphic lines, according to the evolution order of calligraphy (large seal→ small seal→ official script→ regular script→ line script →cursive script), the correlation between calligraphy styles shows a downward trend, and cursive script is negatively correlated with most calligraphy styles.

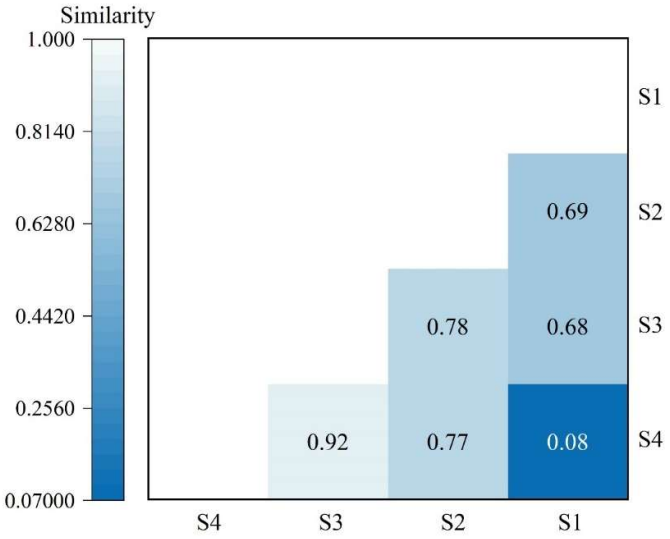

(a)Similarity of calligraphy structure

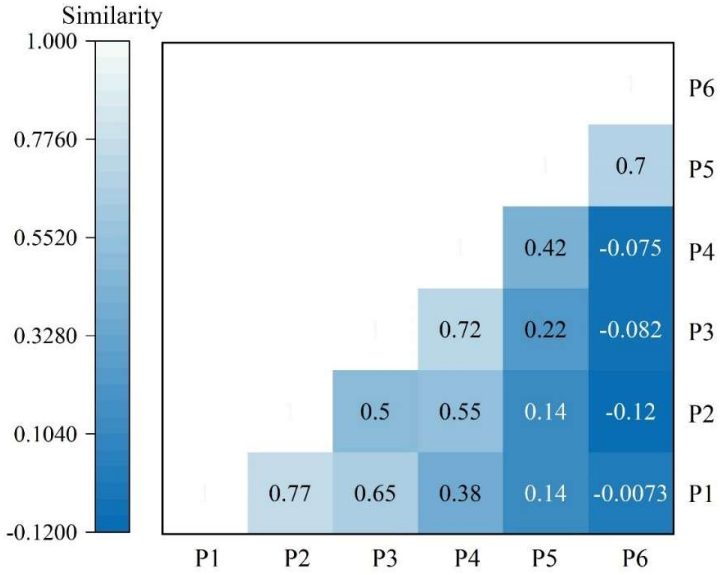

(b)Similarity of lines of calligraphy

Fig. 5. The overall correlation analysis of calligraphy line and structure

4.2.2. Correlation analysis between calligraphic structures under different calligraphic lines. After the above analysis of the overall correlation between calligraphic lines and structures, the correlation is further subdivided, i.e., the correlation between the 4 calligraphic structures under different calligraphic lines and the correlation between the 6 calligraphic lines under different calligraphic structures are calculated respectively, and the former will be analyzed in depth in this section first. The correlation between the four calligraphic structures without the calligraphic lines is shown in Table 2, where the r-value of the highly positive correlation ranges from [0.8,1]. According to the data in the table, it is found that the correlation between the four calligraphic structures is positive under each calligraphic style, and most of the correlations are strong. Further analysis of the correlations shows that compared with the Big Seal Script, Small Seal Script and Clerical Script, there are higher correlations among the 4 calligraphic structures of Regular Script, Running Script and Cursive Script, indicating that the calligraphic styles formed after the Clerical Script are more emphasized on brushwork.

Table 2. The correlation between calligraphy structures

-	-	S2	S3	S4
P1	S1	0.92	0.78	0.58
	S2	-	0.82	0.52
	S3	-	-	0.69
P2	S1	0.94		0.47
	S2	-	0.48	0.57
	S3	-	-	0.38
P3	S1	0.88	0.79	0.88
	S2	-	0.78	0.78
	S3	-	-	0.8
P4	S1	0.98	0.85	0.85
	S2		0.87	0.87
	S3	-	--	0.93
P5	S1	0.96	0.9	0.76
	S2	-	0.82	0.7
	S3	-	-	0.77
P6	S1	0.97	0.88	0.8
	S2	-	0.9	0.86
	S3	-	-	0.85

4.2.3. Correlation analysis between calligraphic lines under different calligraphic structures. In this section, further analysis of the correlation between the six calligraphic lines under different calligraphic structures will be carried out. The correlations are shown in Table 3. From the table, it can be seen that under each type of calligraphic lines, basically all of them are weakly correlated, except for the high correlation between the Big Seal Script and the Small Seal Script, in which the Cursive Script is negatively correlated with some of the calligraphic styles. Regardless of the calligraphic structure, the further apart the calligraphic styles are, the lower the correlation is, indicating that with the evolution of the calligraphic styles, the differences in calligraphic lines between the styles are getting bigger and bigger, and the structure does not interfere too much with this process of change.

Table 3. The correlation between the lines of calligraphy

-	-	P2	P3	P4	P5	P6
S1	P1	0.87	0.7	0.43	0.09	-0.15
	P2	-	0.74	0.54	0.09	-0.22
	P3	-	-	0.72	0.08	-0.21
	P4	-	-	-	0.32	-0.19
	P5	-	-	-	-	0.74
S2	P1	0.76	0.68	0.32	0.02	-0.02
	P2	-	0.67	0.65	0	-0.25
	P3	-	-	0.74	0.1	-0.15
	P4	-	-	-	0.27	-0.15
	P5	-	-	-	-	0.78
S3	P1	0.82	0.45	0.21	0.16	0.16
	P2	-	0.22	0.12	0.16	0.2

	P3	-	-	0.78	0.42	0.06
	P4	-	-	-	0.58	0.16
	P5	-	-	-	-	0.78
S4	P1	0.78	0.72	0.59	0.46	0.08
	P2	-	0.66	0.76	0.35	-0.15
	P3	-	-	0.75	0.58	0.18
	P4	-	-	-	0.66	0.12
	P5	-	-	-	-	0.68

4.3. Significance test for the effect of calligraphic geometric features

At present, there is a lack of aesthetic experience scale suitable for the geometric characteristics of calligraphy, so this experiment selects calligraphic style adjectives from several academic works that are recognized as representative of the geometric characteristics of calligraphy. After screening, a total of 45 style words were extracted as the dimensions of the aesthetic scale, namely: majestic, Xiuyi, quaint, chic, sinister, quiet, spicy, elegant, graceful, bold, rough, mellow, ruthless, dignified, robust, round, crisp, plump, fat, thin, dense, sparse, round, dense, skillful, innocent, fat, square, old, natural, wild, chonghe, calm, vigorous, simple, strange, charming, dangerous, tight, round, stubborn, ancient, broad, quite jun, Elegant. Selected works include Sixteen Lectures on Calligraphy Aesthetics and Criticism, Twenty-Four Books, and History of Chinese Calligraphy Style.

Repeatable two-way ANOVA was used for significance testing because the dependent variable in this experiment was a dichotomous variable, so the ANOVA results needed to be corrected for Huynh-Feldt degrees of freedom. Repeatable two-way ANOVA tests were conducted separately for the 45 style measure terms. The "line" factor was found to be significant ($p<0.05$) in all dimensions except for the five dimensions of Euphemism, Roundness, Lushness, Denseness, and Boldness. However, the "structure" factor was $p \geqslant 0.05$ in 15 dimensions, such as danger, strength, roundness, and abundance, and the effect was not significant. The interaction between the two factors was not significant on the 15 dimensions of majesty, old-fashionedness, elegance, and euphony.

4.4. Experimental results and analysis

1) The importance of calligraphic line and structure to the geometric features of calligraphy. Compared with "structure", "line" has a significant impact on more stylistic dimensions, i.e. "line" has a more significant impact on the geometric features of calligraphy. However, it is worth noting that the geometric features of calligraphy are not completely determined by "lines", and it can also be seen through ANOVA that "structure" also has an influence on some geometric features, and for a small number of geometric feature dimensions, there is an interaction between "line" and "structure".

2) Quantify the differences in geometric features between book styles. Through the hierarchical cluster analysis and correlation analysis above, it can be found that the geometric characteristics of calligraphy are similar between large and small seals, large seals and official scripts, small seals and official scripts, official scripts and regular scripts, and cursive scripts and line scripts, while the similarity between cursive script and the other four calligraphy styles except line script is very low, indicating that the geometric characteristics of cursive script are very unique. The quantitative results are in line with the traditional understanding of book theory.

5. Conclusion

Combined with morphological convolutional neural network MCNN, this study constructs a calligraphy geometric feature recognition model to solve the problem of low recognition accuracy in traditional recognition models. In order to verify the feasibility of the model, calligraphy geometric feature recognition test is carried out. In the recognition detection on the ancient regular script calligraphy dataset, the average

recognition accuracy of this paper's model is as high as 97.23%, which is higher than that of the CNN, LeNet-5, GoogLeNet, and ResNet models that are used as comparisons by 3.88%, 6.48%, 5.68%, and 0.78%. Facing the ancient Regular Script Calligraphy such as Ou Style, Liu Style, Zhao Style, and Yan Style, the recognition accuracy of this paper's model reaches 99.8%, 98%, 96%, and 98.5%, respectively. Overall, it shows excellent performance in recognizing geometric features of calligraphy.

The model of this paper is used to extract experimental data related to calligraphic lines and structures to explore the influence of calligraphic lines and structures on geometric feature styles. In terms of line and structure for overall correlation, the similarity between calligraphic structures is higher overall, while in terms of calligraphic lines, the correlation between calligraphic styles is on a decreasing trend according to the evolutionary order of the styles. The correlations among the 4 types of calligraphic structures under different calligraphic lines are all positive. Among the 6 ancient calligraphies, there are higher correlations among the 4 calligraphic structures of Regular Script, Running Script and Cursive Script compared to Big Seal Script, Small Seal Script and Official Script, indicating that the calligraphic styles after Official Script are more emphasized on brushwork. Under different calligraphic structures, except for the high correlation between the Big Seal Script and the Small Seal Script, the correlations among the other ancient calligraphic types are weak, and the negative correlation between the Cursive Script and all the calligraphic styles except the Running Script. This suggests that as the calligraphic styles evolved, the differences in calligraphic lines between the styles became larger and larger. In general, compared with "structure", "line" has a more significant influence on the geometric features of calligraphy, and among the six types of ancient calligraphy studied, the geometric features of Cursive Script are the most unique, which are only relatively similar to those of Running Script, and very little similar to those of the other four types of ancient calligraphy. The similarity with the other four types of ancient calligraphy is very low.

References

[1] Shi, X. (2023). An Aesthetics of Chinese Calligraphy. Philosophy Compass, 18(5), e12912.

[2] Hung, R. (2024). Self-cultivation through art: Chinese calligraphy and the body. Educational Philosophy and Theory, 56(7), 621-625.

[3] Chen, Z. (2023). Chinese Calligraphy: An Ancient Art in the Modern Era. In SHS Web of Conferences (Vol. 159, p. 02003). EDP Sciences.

[4] Pengcheng, G., Gang, G., Jiangqin, W., & Baogang, W. (2017). Chinese calligraphic style representation for recognition. International Journal on Document Analysis and Recognition (IJDAR), 20, 59-68.

[5] Li, Z. (2017). The Chinese aesthetic tradition. University of Hawaii Press.

[6] Gao, J. (2018). Aesthetics and art: Traditional and contemporary China in a comparative perspective. Springer.

[7] Xu, Y., & Shen, R. (2023). Aesthetic evaluation of Chinese calligraphy: a cross-cultural comparative study. Current Psychology, 42(27), 23096-23109.

[8] Hou, Y. (2024). The Aesthetic Expression of Abstract Calligraphy: Emotion and Form between Brush and Ink. Journal of Ecohumanism, 3(6), 1493-1505.

[9] Kim, D. (2022). A Study on the aesthetic of Calligraphy by Seok Jeon Hwang Wook. The Journal of the Convergence on Culture Technology, 8(2), 227-234.

[10] Kim, D. (2020). The Calligraphy theory and the aesthetic of Calligraphy on Wongyo Lee KwangSa. The Journal of the Convergence on Culture Technology, 6(4), 179-186.

[11] Wang, L., & Hamidon, N. A. (2023). Aesthetic and Value Study of Inscriptions from the Perspective of Calligraphy. Art and Performance Letters, 4(11), 44-49.

[12] Kim, D. (2021). A Study on Calligraphy theory and the Calligraphy and Paintings aesthetic of GangAm, Song

Sungyong. The Journal of the Convergence on Culture Technology, 7(4), 273-280.

[13] Fu, X., & Tho-ard, M. (2023). Imagery Expression And Aesthetic Significance Of Chaptering In Chinese Calligraphy. Journal of Namibian Studies: History Politics Culture, 33, 43-59.

[14] Guxue, L., & hee Luen, L. C. (2024). The Integration of Visual Aesthetics and the Implementation of Innovative Techniques in Chinese University Calligraphy Education. Asian Journal of Research in Education and Social Sciences, 6(3), 828-834.

[15] Shi, X. (2019). Chinese calligraphy as "force-form". Journal of Aesthetic Education, 53(3), 54-70.

[16] Matsumoto, K., & Okada, T. (2021). Imagining how lines were drawn: The appreciation of calligraphy and the facilitative factor based on the viewer's rating and heart rate. Frontiers in human neuroscience, 15, 654610.

[17] Zhang, Y., Chen, L., Chen, H., Chu, J., Chang, B., Wang, Y., & Sun, G. (2023). Visual analysis of inscriptions in the Tang Dynasty: a case study on the calligraphy style of Wang Xizhi. Visual Intelligence, 1(1), 8.

[18] Li, R., Jia, X., Zhou, C., & Zhang, J. (2022). Reconfiguration of the brain during aesthetic experience on Chinese calligraphy—Using brain complex networks. Visual Informatics, 6(1), 35-46.

[19] Zhou, P., Zhao, Z., Zhang, K., Li, C., & Wang, C. (2021). An end-to-end model for chinese calligraphy generation. Multimedia Tools and Applications, 80, 6737-6754.

[20] Wang Zhen,Liu Ying,Du Jinsong,Wang Zheng & Shao Qihe. (2022). De-noising magnetotelluric data using variational mode decomposition combined with mathematical morphology filtering and wavelet thresholding. Journal of Applied Geophysics.

[21] Zhang Xiaochen,Cong Yiwen,Yuan Zhe,Zhang Tian & Bai Xiaotian. (2021). Early Fault Detection Method of Rolling Bearing Based on MCNN and GRU Network with an Attention Mechanism. Shock and Vibration

[22] Takahiro Kushida,Ryutaro Nakamura,Hiroaki Matsuda,Wenhao Chen & Kenichiro Tanaka. (2024). Affine transform representation for reducing calibration cost on absorption-based LWIR depth sensing. Scientific Reports(1),26429-26429.

[23] Abderrahim Charkaoui,Anouar Ben Loghfyry & Shengda Zeng. (2024). Nonlinear parabolic double phase variable exponent systems with applications in image noise removal. Applied Mathematical Modelling495-530.